

Antennas for 5G-NR Communications Via Satellite

Carolina Isabel Martins Espada
carolina.espada@tecnico.ulisboa.pt

Abstract—A Radial Line Slot Array (RLSA) antenna is developed for 5G and Satellite-on-the-move (SOTM) applications. These antennas are highly directive, low-cost, low profile and can be circularly polarized. Beam steering in elevation and azimuth, which is also fundamental for next generation of millimeter wave communications, is the key requirement that shapes the developed RLSA. In this work, the RLSA is envisioned to be part of an antenna composed by a stacked transmit-array (TA) and RLSA, based on the Risley prism configuration. The additional degree of freedom provided by the phase correction of the TA, allows exploring new RLSA layouts. Starting from a RLSA design for boresight beam and a tilted beam collimation cases, and ending with a new RLSA slot arrangement that generate an offset spherical-like out-going wave. Cascading this last RLSA design with a properly design TA provide a new way of implementing the Risley prism-based antenna – which is one innovative aspect of this work. A RLSA prototype was fabricated with a total thickness of 11.61 mm and an aperture diameter of 150 at 30 GHz. The operation bandwidth is quite large for this type of antenna [28.4, 30.1 GHz] mostly due to the optimized feed cavity that was developed for this antenna, which proved to be much easier to fabricated than conventional solutions. Numerical simulation shows that the RLSA together with the TA provide good performance in terms of X-pol (< -15 dB), SLL (< -10 dB) and scanning range (up 53° degrees in elevation with scan loss below 3dB).

Index Terms—5G-NR, Beam Steering, CP-RLSA, Risley Prism, SOTM.

I. INTRODUCTION

SHARING information between different parts of the world is a quick and easy task. However, for moving platforms, these connections cannot be made easily and a working solution is required. Millimeter wave (mm-wave) are used in 5G and Satellite-on-the-move (SOTM) applications, such as Low Earth Orbit (LEO) and Medium Earth Orbit (MEO) satellites. Due to the distance between the ground and the space, and the mobility of 5G users and SOTM, a strong and scanning connection is necessary. The high-gain antennas are the indicated ones to work on mm-wave, such as parabolic antennas or phased arrays. However, the first occupy a substantial volume, meanwhile the phased arrays have a considerable energy consumption and are expensive. Therefore, mm-wave applications need a more reliable solution. An alternative to overpass the problems mentioned are the low-profile, low-weight, and low manufacturing costs.

A more appealing solution is a RLSA antenna, which have a planar profile and highly directive radiation characteristics. RLSA belongs to a class of slotted waveguide antennas, formed by a Parallel Plate Waveguide (PPW). A probe-like feed, placed in the bottom plate, excites a radial TEM travelling wave that leakage through the slots crafted in the

upper plate. RLSA antennas can be designed for both linear and circular polarization.

In 1963, K. Kelly and F. Goebels describe RLSA antennas that can operate using circular, linear, or elliptical polarization through an adjustment in the feed circuit [1]. In 1985, Ando et al. developed a double layer CP-RLSA and presented mathematical equations to distribute the slots spirally on the upper plate of the antennas [2]. Years later, the same author presented a double-layer linearly polarized (LP-RLSA) [3]. A double layer RLSA permits a uniform aperture illumination and reduces the terminated power loss. However, it has problems dealing with the remaining power, leading to low efficiency and gain. Therefore, in 1990, Ando et al. innovated and introduced a single-layered CP-RLSA [4], which is much simpler to fabricate. The drawbacks compared to a double layer RLSA, such as the terminated loss is high and the aperture field is steeply tapered. To overcome these problems, the authors propose new techniques to improve the antenna performance. The first one consists of non-uniform slots, i.e, slot length, and their spacing may vary over the aperture to realize uniform illumination. The other one consists of adding a matching spiral to radiate the residual power at the perimeter of the antenna to suppress reflections at the feeder. In 1995, Takashi et al. proposed a beam tilting RLSA, the center of the spiral is biased to radiate in the main beam direction [5]. The beam tilt technique is interesting because it permits the choice of the desired direction, without having a broadside beam. Starting in 2000, researchers focused on computational solutions to find an ideal design. In 2003, M. Sierra-Castañer et al. proposed a method for medium and high gain CP-RLSA antennas by determining the position and length of the slot pairs by a systematic design to optimize the co-polar to cross-polar ratio [6]. In 2012, M. Albani et al. developed a computational method that reduces the distortion of the radiation pattern. The three prototypes present a good performance, working at 22 GHz [7]. Lately, Koli et al., have been studying in depth to improve the performance of the RLSA. The authors presented CP-RLSA designs with the waveguide fully and partially filled with dielectric materials and fully filled with air [8], [9]. Morales et al. using the technique in [7] and the theory in [6], developed an optimization technique to control the amplitude and phase of the slots [10].

Recently, Afzal et al. proposed a beam steering of fixed high-gain antennas, where two rotating metasurfaces are placed above a CP-RLSA antenna in the near field region. By rotating both metasurfaces, the beam can be steered in any direction [11], [12]. Z. Zhang implements the Risley prism concept and can steer the beam using just a single metasurface by rotating the leaky-wave antenna and the upper Transmit Array (TA) [13].

¹C. Espada is with Instituto Superior Técnico, Lisboa, Portugal.

This work focuses on the development of a rotating system composed of an RLSA and a TA, in which their phase distributions complement each other, as the RLSA can act as a base for a TA to tilt the beams. Hence, the antenna scans a pencil beam shape directed in a selected direction, with high directivity and has lower SLL compared to current solutions. Therefore, slot size, position, and orientation have a strong influence on antenna performance. The TA placed above the RLSA does not interfere with the electrical field magnitude emitted through the antenna, but with the phase distribution.

In the rest of the paper, first, the RLSA formulation theory and methodology are described, afterwards, it is presented how antenna parameters influence the antenna performance. Lastly, the simulations results obtained for the final set up are presented, along with their discussion.

II. FORMULATION

A. PPW - Parallel Plate Waveguide

The RLSA structure consists of a circular parallel plate waveguide (PPW) fed at the center of the lower waveguide. One common feed approach is to use a coaxial cable to excite an outward traveling wave that propagates between the parallel plates in the radial direction. The mode inside the waveguide excites the slots on the upper plate that radiate part of the propagating power, as expected from a leaky wave antenna. Figure 1 shows the behaviour of the wave inside the RLSA.

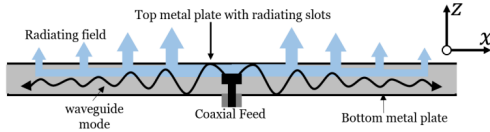


Fig. 1. The travelling wave inside the waveguide. [14]

When developing a RLSA antenna the height of the waveguide has to be chosen carefully because it defines which modes operate inside the waveguide. The operation of the RLSA requires monomodal operation with the fundamental cylindrical model $TM_{0,0}^z$, corresponding to the condition [7]:

$$h < \frac{\lambda_g}{2} \quad (1)$$

Where h is the distance between the plates and λ_g is the guided wavelength. The wavelength propagating inside the PPW is given in (2), which relates the guided wavelength with the free-space wavelength, and the relative electrical permittivity, ϵ_r [10].

$$\lambda_g = \frac{\lambda_0}{\sqrt{\epsilon_r}} \quad (2)$$

The radius of the RLSA is also an important parameter. The aim is to radiate all the power along the waveguide and have lower power at the perimeter of the RLSA. The larger the radius, the RLSA will have more elements and more power escapes through them. Consequently, the antenna will have less residual power at the end of PPW. On the other side, aperture antennas with a small radius tend to have poor return loss performance. Therefore the energy that arrives at the edge must be absorbed or radiated to not spoil the antenna performance.

B. Feeder Structure

There are different feeding approaches for this type of antennas that can be double-layer [2] or single layer [4]. In the first case, that is more complex to fabricate, the PPW operates with an inward radial wave, whereas in the single layer case, an outgoing radial wave is excited usually using coaxial cable probes. Cable depth can significantly influence antenna performance, so its control must be precise. Since these antennas can reach small heights, it becomes difficult to adjust the position of the cable within the waveguide.

Instead of having a coaxial cable directly inserted into the waveguide, as the single-layer structure, it is used a small open-end cavity that couples the coaxial feeding to the lower plate. Fig. 2 shows the structure. The cavity is a circular aperture to carry radial waves. Two important parameters when sizing the cavity are its radius and height. Relatively to the radius, it is limited by the position of the first pair of slots. Meanwhile, the height follows the same rule as (1), to allow only the fundamental cylindrical mode $TM_{0,0}^z$. The cavity is filled with air, thus the free-space wavelength propagates inside it.

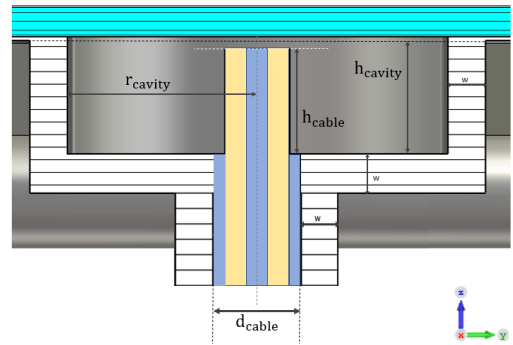


Fig. 2. RLSA feeding structure used. The dimensions are represented by the following variables: r_{cavity} - radius of the cavity, h_{cavity} - height of the cavity, h_{cable} - cable depth inside the cavity and d_{in} - diameter of an opening for cable insertion.

C. Aperture distribution - Plane wave

The slots are designed to couple with the radial currents flowing over the upper plate. The magnetic field inside the PPW is obtained through the Hankel function of the second kind of order one [9]:

$$H_\phi(\rho) = H_1^{(2)}(k_g \rho) \approx \sqrt{\frac{2}{\pi k_g \rho}} e^{-j(k_g \rho - 3\pi/4)} \quad (3)$$

where $k_g = 2\pi/\lambda_g$ is the wavenumber in the radial waveguide and ρ is the radial position.

The slots in a pair are placed in order to perform circularly polarized wave, to accomplish it there are three conditions. To begin with, the field must have two orthogonal linear components. Furthermore, the two components must have the same magnitude, and lastly, the components must have a time-phase difference of odd multiples of $\pi/2$ radians [15]. Figure 3 illustrates the slot distribution to achieve RHCP (Right hand circular polarization), to have LHCP (Left hand circular polarization) a rotation of 90° is required in each slot.

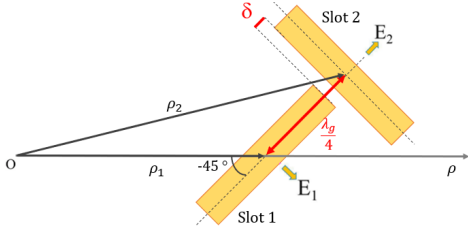


Fig. 3. Two orthogonal slots placed to achieve RHCP

Relative to the conditions mentioned above, each slot in a pair produces a linear component. These components have the same magnitude if both slots have the same length and width. Relatively to the phase difference condition, the following equation needs to be satisfied [2]:

$$\arg(H_1^{(2)}(k_g \rho_2)) - \arg(H_1^{(2)}(k_g \rho_1)) = \frac{\pi}{2}, \quad (4)$$

where ρ_1 and ρ_2 are the radial distance between the middle of the slots and the center of the aperture. The argument of $H_1^{(2)}$ is described in (3). Therefore, solving (4), the minimum distance between two orthogonal slots is [9]:

$$\rho_2 - \rho_1 = \frac{\lambda_g}{4} \quad (5)$$

Slot pairs density over the aperture is defined as $S_\phi \times S_\rho$. S_ρ is the radial spacing between slot pairs while S_ϕ is the azimuthal distance between adjacent slot pairs [2]. Every azimuthal rotation adds a phase factor, $e^{-j\phi}$, which is a compensation to feed in phase all the slots [2], therefore S_ρ is defined as the guide wavelength and λ_g . S_ϕ is defined arbitrarily.

Boresight Beam

The following equations describe the slot arrangement process to obtain a directive beam perpendicular to the antenna plane. If $k\rho \gg 1$, according to [2], the angle of rotation for each slot pair can be simplified to:

$$\rho_s(\phi) = \rho_1 + \phi \frac{\lambda_g}{2\pi} \quad (6)$$

An expansion can be made for (6) to obtain the angle of rotation for each slot pair for an arbitrary arc length. The parameters θ_1 and θ_2 are the inclination angles with the radial direction, ρ . For an arbitrary angular interval between them, the corresponding arc length can be calculated through the integral below [16]:

$$\text{arclen} = \int_{\theta_1}^{\theta_2} \rho_1 d\phi + \frac{\lambda_g}{2\pi} \int_{\theta_1}^{\theta_2} \phi d\phi \quad (7)$$

Solving in order to θ_2 using a simple quadratic formula, we obtain the following expression [16]:

$$\theta_2(\theta_1) = -k_g \rho_1 + \sqrt{(k_g \rho_1)^2 + 2k_g \text{arclen} + 2k_g \rho_1 \theta_1 + \theta_1^2} \quad (8)$$

where arclen represents the azimuthal distance between two radiating slot pairs, thus corresponding to the aforementioned variable, S_ϕ . This value is the same for consecutive slot pairs along the spiral. Figure 4 (a) shows the spiral where the pair of slots must be placed to perform a boresight beam.

Beam tilted distribution

By changing the distribution of the slots, it is possible to tilt the planar wave instead of a boresight one. In a biased elongated spiral, the slots position should follow [5]:

$$\rho_s(\phi) = \frac{\phi}{k_g - k_0 \sin \alpha_0 \cos \phi} \quad (9)$$

Where k_g and k_0 are the guided and free-space wavenumbers, respectively, inside the PPW. The parameter α_0 corresponds to the angle chosen for the tilt.

As Fig.4 illustrates, when the beam is tilted, the right side of the RLSA has fewer slots than the left side. Due to the proximity of the slots on the left, it must be ensure that they do not overlap, while on the right they must not be further apart.

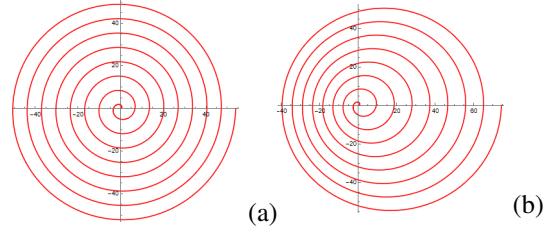


Fig. 4. Slot arrangement for: Boresight Beam (a) and Beam Tilted (b)

D. Aperture distribution - Sub-spherical Wave

In this subsection, we propose an RLSA with a new phase distribution, this phase is complemented with the TA phase correction above, realizing the Risley Prism concept. To have a plane wave escaping through the RLSA+TA antenna, the type of wave released by the antenna is neither plane nor spherical, let's define it as a sub-spherical wave. Similar to what happens in Fig. 5 (a), but in our case, the feed horn plus the first prism corresponds to an RLSA antenna, and the second flat prism is a TA, that does a phase correction. Either the RLSA and TA can rotate independently, having a rotation angle defined by ψ_1 and ψ_2 , respectively. Figure 5 shows the referred angles, the differential rotation angle ξ and the mean rotation angle ϕ . According to [17]:

$$\begin{aligned} \xi &= \frac{\psi_1 - \psi_2}{2} \\ \phi &= \frac{\psi_1 + \psi_2}{2} \end{aligned} \quad (10)$$

The phase distribution inside the PPW is given by:

$$\phi_{PPW}(\rho, \phi) = k_0 \sqrt{\epsilon_r} \rho - \phi \quad (11)$$

The first term corresponds to the phase of a spherical wave. The rotation of the slots to perform the CP introduces an additional phase, to compensate for it, the term ϕ is introduced, which corresponds to the azimuth angle. The phase distribution within the PPW is difficult to control, therefore, what is controlled is the phase distribution of the wave released from the RLSA. The leaky-wave antenna tilts the output spherical wave with an elevation angle α_0 and generates a virtual focus

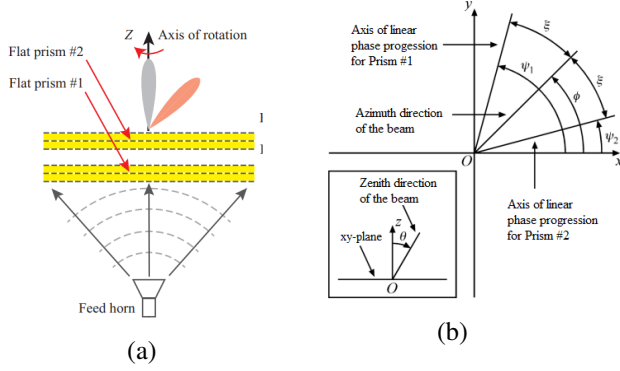


Fig. 5. Configurations for the Risley Prism concept [13]. System with a feed horn and two Flat Prisms (a). Rotation angles, ψ_1 and ψ_2 , seen from the azimuth plane [17] (2).

F_2 that increases the directivity. Hence, the desired phase distribution for the first transmit array is presented as:

$$\phi_{out,1}(\rho, \phi) = k_0 \left[\sqrt{\rho^2 + F_2^2} + \rho \cos \phi \sin \alpha_0 \right] \quad (12)$$

To find the correct position of the slots, (11) and (12) are cancelled out. Figure 6 illustrates the points where the slots will be placed. We can see that with the sub-spherical wave method, Figure 6, have less radiator units for the same area than those shown in Fig.4.

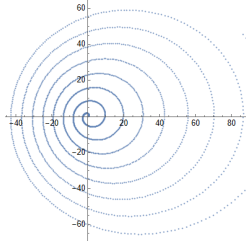


Fig. 6. Set of point where the desired phase wave is equal to the phase inside the PPW

At this stage, a sub-spherical wave is produced. The TA above the RLSA is responsible to perform a plane wave, tilting the wave coming from the RLSA by an offset angle α_0 and finally producing a collimated beam. The TA phase delay for a rotation angle ψ_2 is given, in Cartesian coordinates, by:

$$\begin{aligned} \phi_{TA,2}(x, y) &= \phi_{out,2}(x, y) - \phi_{in,2}(x, y) \quad (13) \\ &= k_0 \left[-\sqrt{x^2 + y^2 + (F_2 + d)^2} + \sin \alpha_0 (\cos \psi_2 x + \sin \psi_2 y) \right] \\ &\quad + k_0 (F_2 + d) \end{aligned}$$

Parameter d is the distance between the RLSA and TA. Once $\phi_{in,2}(x, y, z) = \phi_{out,1}(x, y, z + d)$, and $F_2 \gg d$, then (13) can be rewritten:

$$\begin{aligned} \phi_{TA,2}(x, y) &= k_0 F_2 + \quad (14) \\ &+ k_0 \left[-\sqrt{x^2 + y^2 + F_2^2} + \sin \alpha_0 (\cos \psi_2 x + \sin \psi_2 y) \right] \end{aligned}$$

Therefore, $\phi_{out,2}$ corresponds to the phase distribution of a plane wave that is produced from the whole set, realizing the Risley Prism concept written in (15),

$$\begin{aligned} \phi_{out}(x, y) &= \phi_{out,2} = \phi_{in,2} + \phi_{TA,2} \quad (15) \\ &= k_0 \sin \theta_{RP} [\cos \phi + \sin \phi y] \end{aligned}$$

where θ_{RP} represents the output elevation angle and ϕ is the azimuth angle. At this point a pencil beam shape with high directivity and low sidelobes is expected from the antenna. θ_{RP} is defined as:

$$\theta_{RP}(\xi) = |\arcsin(2 \sin \alpha_0 \cos \xi)| \quad (16)$$

E. Methodology

Numerical methods are based on Geometric Optics/Physics Optics (GO/PO) analysis using KH3Dslot, which is a *Wolfram Mathematica* script. This script is responsible for placing the slots on the upper plate of the antenna. It uses (6) and (9), for a boresight beam and a beam tilted, respectively. When a subspherical wave is desired, KH3Dslot is based on (12).

The connection between KH3Dslot and CST software is made with a VBA macro. Once in CST, a full wave analysis of the model is made, such as return loss, radiation patterns of the directivity, co and cross polarization.

Finally, to analyze the Risley Prism results of the RLSA+TA set, RLSA_TA is used together with the KH3D_near program, also based on GO/PO and a *Wolfram Mathematica* script. Nearby fields are extracted from CST with a cut in a given z-plane. Then the script reads the fields and calculates the phase distribution of the wave released from the RLSA, $\phi_{in,2}$. Finally, it uses the phase correction of TA (II-D) to obtain the final phase distribution (15), thus producing the Risley Prism concept. KH3D_near calculates the near and far-field radiation of the antenna.

III. SIMULATION RESULTS AND DISCUSSION

A. PPW and Cavity Optimization

For first approach, a conical flare at the edge of the plates is considered and the waveguide is filled with a dielectric substrate - Duroid 5880. With the introduction of the flare, the radiated energy at the perimeter of the PPW, will not affect the energy emitted through the slots on the upper plate and lower energy reflected back at the feed is expected. Both upper and bottom plate are considered perfect electrical conductors and start with a thickness of 0.1 mm, and the dielectric thickness is 1.575 mm. The use of a dielectric decreases the guide wavelength, allowing for more radiator units on the top plate of the RLSA, hence increasing the antenna performance. The PPW have a radius of 75 mm and the dielectric have 78 mm radius. To feed the antenna, a cavity is used. After several simulations, the dimensions that provide a good return loss across the frequency band was for $r_{cavity} = 5$ mm, $h_{cavity} = 3$ mm and $h_{cable} = 2.7$ mm, as illustrated in Fig. 7. The coaxial cable inserted in the cavity is EZ-86.

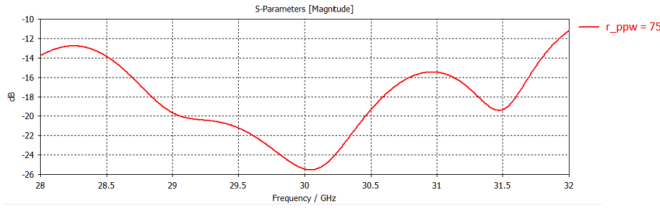


Fig. 7. $S_{1,1}$ for $r_{ppw} = 75$ mm with $r_{cavity} = 5$ mm, $h_{cavity} = 3$ mm and $h_{cable} = 2.7$ mm.

B. Aperture Design - Plane wave

When designing the slots, for their dimensions were considered a width of $\lambda_g/20$ while the length was $\lambda_g/2$. Two type of RLSA are studied, the former produces a boresight beam, while the latter tilts the beam with an offset angle $\alpha_0 = 24^\circ$. The slots are distributed to achieve RHCP as co-pol.

When $\alpha_0 = 0^\circ$, the antenna has achieved a peak broadside directivity of 26.6 dBi with an aperture efficiency of 20.8% at 29.5 GHz. The other antenna has shown a peak directivity of 26.4 GHz and an aperture efficiency of 20.6% at 29 GHz. The directivity did not changed significantly between the two models. The axial ratio (AR) was obtained from CST, where for both CP-RLSA antennas it is less than 3 dB for across the studied frequency band, which is a good indicator to perform CP. Figure 8 illustrates the 1D CST view of the directivity radiation patterns of the two CP-RLSA antennas at 29.5 GHz and 29 GHz, when $\phi = 0^\circ$. Both prototypes have a good performance from 28.5 GHz to 29.9 GHz.

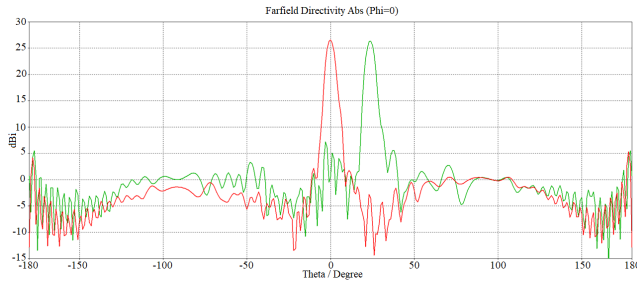


Fig. 8. Farfield Directivity 1D Radiation Pattern when $\varphi = 0^\circ$ at: 29.5 GHz for $\alpha_0 = 0^\circ$ (red) and 29 GHz for $\alpha_0 = 24^\circ$ (green)

Table I shows the comparison of this work with recent and identical researches [8], [9], [18], [19]. It demonstrates that this design has the worst aperture distribution, although it is the one with the best total and radiation efficiency. The position of the slots, dimensions and orientation of the angles need to be studied in the future to increase the aperture efficiency. However, a progress in terms of total and radiation efficiency is noticed, but remember that the structure still has a flare that can influence the results. Without the flare, the energy that is escaping through it would interfere in other directions, spoiling the results.

Finally, the near fields are extracted from CST at {28.5, 29, 29.5, 30} GHz and tested with the implementation of the Risley Prism concept. The frequencies chosen are related to the frequency range that the designs work best. A frequency of 30 GHz is also chosen once is the central operating frequency.

TABLE I
COMPARISON OF RESULTS WITH PREVIOUS STUDIES [8], [9], [18], [19]
FOR BORESIGHT BEAM ($\alpha_0 = 0^\circ$)

$\alpha_0 = 0^\circ$	[18]	[19]	[8]	[9]	This work
Diameter [m]	$26.8\lambda_0$	$6.5\lambda_0$	$16\lambda_0$	$27\lambda_0$	$15\lambda_0$
Permittivity ϵ_r	2.2	2.2	2.2	1	2.2
SLL	-17.4	-12.8	-11.2	-16.8	-15.1
X-Pol [dB]	-	-	-	-24.5	-38.95
e_a [%]	59.6	40	38.3	56	20.8
Total Effic. [%]	95	93	-	95.4	97.44
Radiation Effic. [%]	-	94	-	97.4	98.18

The cuts to extract the fields are made in the $z = 9$ plane, so the flare not interfere, then the cut has to be above its height. RLSA_TA, is used to calculate the phase distribution of the RLSA on the cutted plane, and evaluates the results with the contribution of the phase delay distribution of TA. Since RLSA has already emitted a plane wave, the TA must have a phase distribution of a plane wave to not disturb it, identical as the equation (15). The TA always steers the beam with the same offset angle α_0 as the RLSA. When α_0 is equal to 0° , then the direction of the main lobe is always perpendicular to the plane of the RLSA+TA. Even if we rotate the elements independently the beam is still pointed to $\theta = 0^\circ$. Meanwhile, when the beam is tilted by an offset angle α_0 , TA_2 also tilts the wave. According to (10), the beam reaches the θ_{max} when $\xi = 0^\circ$, oppositely $\theta_{RP} = 0^\circ$ when $\xi = 90^\circ$, ξ depends on the rotation angles, ψ_i . A direct comparison between RLSA-Ta and CST results cannot be made, as the former is based on approximations and overestimates the results. However, the best frequencies agree with the ones obtained in CST.

C. Aperture design - Sub-spherical Wave

In this section, the objective is to build an antenna using the method explained in subsection D of the Chapter II. Formulations. The offset angle is $\alpha_0 = 24^\circ$, so the beam produced by the RLSA+TA has a maximum theoretical angle of $\theta_{RP} = 54^\circ$ with respect to the normal direction. Various solutions are tested to decrease the energy at the perimeter of the RLSA and also the cross-polarization. TA is 5 mm above the RLSA antenna. RHCP is also the co-pol. The farfield obtained at 30 GHz is illustrated by Fig. 9, when $\varphi = 0^\circ$.

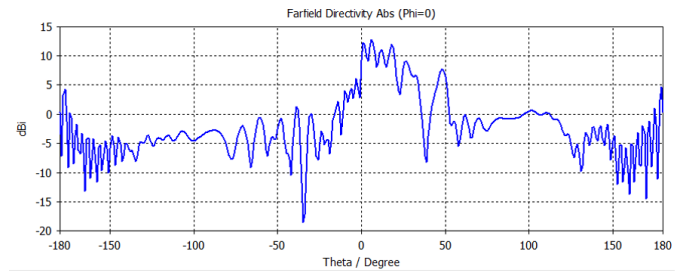


Fig. 9. Farfield Directivity 1D Radiation Pattern at 30 GHz with $\varphi = 0$ and $\alpha_0 = 24^\circ$ (blue)

Comparing Fig. 8 with Fig. 9, it is clear there is a big difference between both images. In this subsection, the RLSA does not produce a collimated beam, but a sub-spherical wave

instead. The studies of the subsection III-B are important because they allowed better visualization of the RLSA conduct with the cavity, instead of the result in Fig. 9, where it is difficult to conclude.

Following the same process as before, the CST fields are also extracted when $z = 9$, and evaluated with the RLSA_TA script. Fig. 10 illustrates that our slots distribution implementation has worked with the phase compensation made by TA, performing the Risley Prism concept. For a better synthesis of the results, we make a comparison of SLL in Table II, from the results obtained from RLSA_TA between a collimated beam tilted and this solution, sub-spherical wave. A confirmation is needed that our new solution has advantages in SLL. Normally, a boresight beam has a higher directivity than a beam tilt, due to scan loss. Therefore, for a more credible comparison, it is only compared when the waves have $\alpha_0 = 24^\circ$, either for a plane or sub-spherical wave. Analyzing Table II, for the majority of the frequencies studied, the sub-spherical wave has in fact presented better SLL, achieving the mian objective of this investigation.

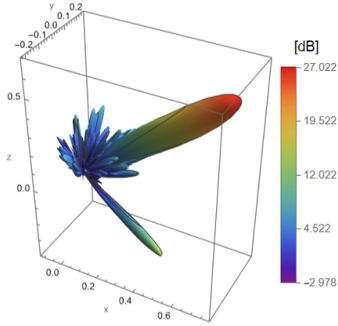


Fig. 10. RLSA_TA Farfield Directivity Radiation Pattern at 30 GHz for sub-spherical wave: $\xi = 0^\circ$

TABLE II
COMPARISON OF RLSA_TA SLL RESULTS FOR A PLANE AND SUB-SPHERICAL WAVE WITH $\alpha_0 = 24$

SLL	Plane wave		Sub-spherical wave	
	$\xi = 0^\circ$	$\xi = 90^\circ$	$\xi = 0^\circ$	$\xi = 90^\circ$
28.5 GHz	-17.5	-17.2	-20.2	-18.9
29.0 GHz	-20.3	-20.1	-20.0	-15.0
29.5 GHz	-20.4	-17	-20.7	-18.7
30.0 GHz	-16.7	-10.3	-18.3	-13.9

Still with the flare, we change the spacing between the pairs of slots in the PPW. We have been working with $arlen = 0.625\lambda_g$ from equation (8). Since the slots are very close to each other, they may couple between them affecting negatively the antenna performance. Therefore, a solution with $arlen = 0.833\lambda_g$ is tested. Doing a depth evaluation through CST, we investigate the θ direction of the main lobe, which is 6° for both solutions. Then, we calculate X-Pol through the values of LHCP minus RHCP in that direction, for each solution. As a result we obtained a X-Pol equal to -22.1 dB and -17.2 dB for $arlen = 0.625\lambda_g$ and $arlen = 0.833\lambda_g$, respectively. Therefore, having higher space between slots

does not correspond to a better cross-pol. In the following subsections, we proceed with the initial solution.

PPW Structures

From now on, the flare is removed from the structure, once it occupies a large volume, but mainly because its fabrications is complex. Therefore a new solution is needed, to replace the flare, once the flare decreases the amount of energy reflected at the feed. The dielectric has the same radius as the PPW, i.e., changes from 78 mm, to 75 mm. Three solutions are studied.

Starting with the first solution, that is a matching spiral (MS) at the back plate of the antenna, has to be placed carefully. Once, the closer to the edge, the more energy will have been released earlier by the pairs of slots, leaving less energy for the continuous slot to extract. Therefore, the matching spiral is placed as far away from the center as possible, and at the same time must not be just below the slots pairs of the top plate, to not steal the energy that can escape through them. MS follows a phase distribution as (6), different from the distribution of the pair of slots. The width of the continuous spiral must not be too large, to not cause reflection at the feed, on the contrary, it must not be too narrow because it does not fulfill the objective, which is to reduce the energy that previously escaped by the flare. The matching spiral width needs more study and improvement, although for our studies it is chosen according to the height of the dielectric, thus $W_{MS} = 1.575$ mm. Fig. 11 (a) shows the bottom plate of the PPW structure when a matching spiral is used.

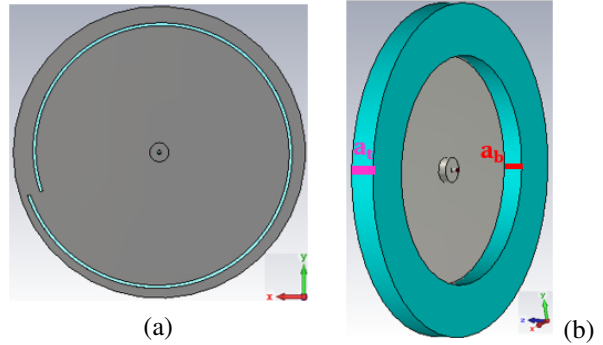


Fig. 11. PPW structure with a: matching spiral in the bottom plate (a); an absorber surrounding the plates (b)

Furthermore, an absorber (AB) is utilized to diminish the reflections. The material chosen is ECCOSORB AN-77. Fig. 11 (b) represents the PPW when it has an absorber rim at the edge of the plates and the variables absorber thickness from the bottom plate, $a_b = 10$ mm, and upper plate, $a_t = 11.775$.

The las solution is a junction of the previous two presented, i.e., a PPW with a matching spiral in the bottom plate, and an absorber rim. In addition to the absorber on the edge of the PPW, it also surrounds the matching spiral for the same purpose, to contain the reflections. Fig. 12 illustrates both solutions together, from a upside view (a) and downside (b).

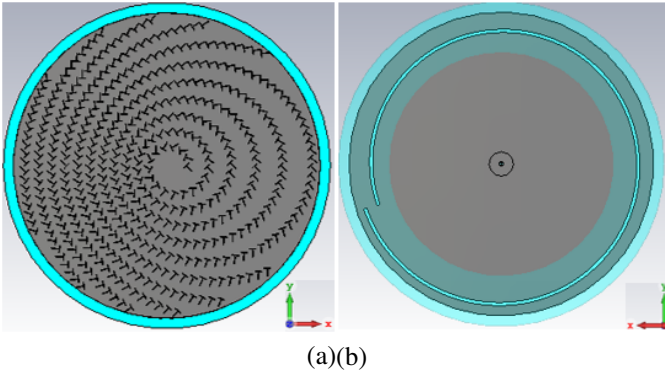


Fig. 12. PPW with absorber and matching spiral: upside plane (a) and downside plane (b)

Fig. 13 compares the reflections coefficients of the three cases mentioned. Analyzing the graphic, a good level of $S_{1,1}$ is achieved for all cases, except for lower frequencies, where the first and second case have internal reflections higher than -10 dB.

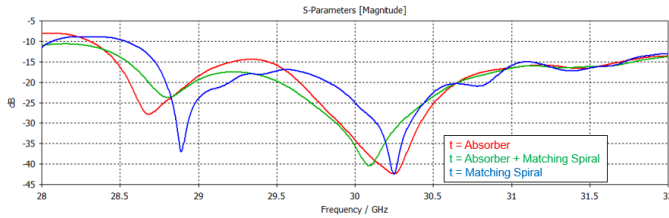


Fig. 13. $S_{1,1}$ for PPW: with absorber (red), absorber + matching spiral (green) and a matching spiral (blue)

Fig. 14 shows the farfield directivity at 30 GHz when $\phi = 0^\circ$, for the three cases when RHCP (a) and LHCP (b). The most important θ directions are $\pm 90^\circ$ and $\pm 180^\circ$. When $x > 0$, where there are less slots, $\theta = 90^\circ$, inversely, the side with more pair of slots, $x < 0$, θ corresponds to -90° . Therefore, since those angles correspond to the edge of the RLSA, they must be as lower as possible. Relatively to $\theta = \pm 180^\circ$ represents how much is emitted at the rear of the antenna.

As proved in Fig. 14, the worst case in the major of the directions is the MS case. It is expected, since it does not have an absorber around the PPW to contain the reflections, then the radiation in both polarizations is higher at the rear. Comparing the other 2 cases, they both have good and similar results. To analyze the best structure for the antenna that we will proceed with, we only compare the results of the RLSA_TA for the AB and MS+AB cases. As the MS case has the worst CST results, it is not expected to improve performance in RLSA_TA over the other cases. Table III compares the values obtained when $\xi = 0^\circ$ and $\xi = 90^\circ$.

From Table III, the directivity difference is not significant, in both ξ values. Nevertheless, the solution with only the absorber has poorer X-Pol and SLL. Considering that controlling the cross-polarization is not a simple task, the solution with the best cross-pol is the one with a matching spiral plus an absorber. The AB+MS case presents better results overall, hence this is the RLSA structure we adopted for the next studies.

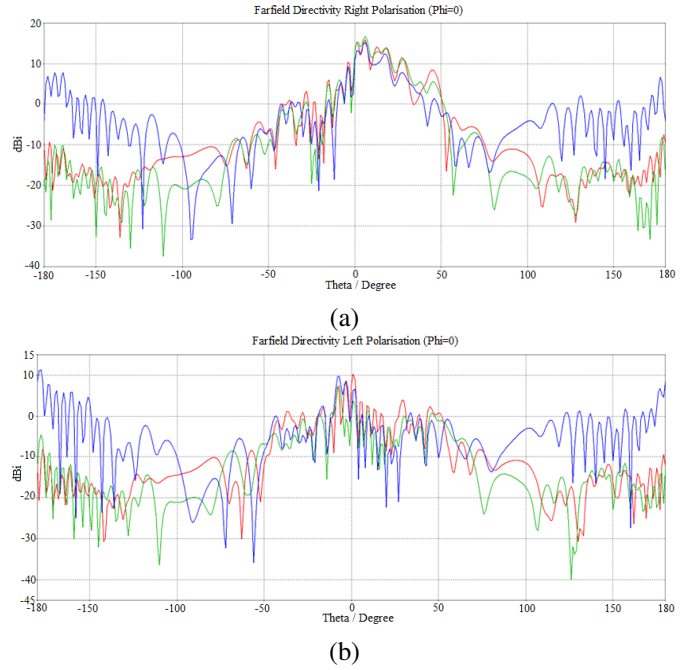


Fig. 14. CST Farfield Directivity Radiation Pattern when $\phi = 0^\circ$ at 30 GHz with AB (red), AB+MS (green) and MS (blue): RHCP (a) LHCP (b)

TABLE III
COMPARISON RLSA_TA RESULTS BETWEEN A STRUCTURE WITH AB AND AB+MS AT 30 GHz FOR: $\xi = 0^\circ$ (A) $\xi = 90^\circ$ (B)

	(a)		(b)		
$\xi = 0^\circ$	AB	AB+MS	$\xi = 90^\circ$	AB	AB+MS
Dir. [dB]	26.6	26.5	28.2	28.5	
X-Pol [dB]	-30.6	-41.4	-16.9	-19.1	
SLL [dB]	-18.1	-19.1	-13.7	-14.8	
e_a [%]	20.6	20.1	30.1	31.7	

Once the best structure has been found and we are getting closer to the final result, the thickness available for the waveguide plates is 0.017 mm, thus influencing the results. The IV table demonstrates the differences in the final results when such switch is made.

Slot Width Variation

A slot width variation is tested, to verify how much it influences the directivity and SLL. As the wave approaches the edge of the RLSA, it becomes weaker, since it has already largely been radiated by the slots in the most central area. The idea is to start with slots thinner at the beginning of the spiral and ending with larger slots. The width range must be chosen carefully, as on the right side of the PPW ($x > 0$), the placement of the slots is very close. Fig. 15 illustrates the PPW with the slots width increasing, also the red rectangle shows a critical zone. That critical zone controls the maximum width of the slots, once they must not overlap, and the slots in the red rectangle are very close to each other. To not have problems with overlapping, several tests were made and the width of the first pair of slots must begin in $W_s = 0.15$ mm, and every 40 pair of slots, the width increases $50 \mu\text{m}$, once it is the maximum precision of the photolithography process, which is

TABLE IV
RLSA_TA RESULTS AT 30 GHZ FOR PLATES THICKNESS OF: 0.1 MM (A)
0.017 MM (B)

(a)		
0.1 mm	$\xi = 0^\circ$	$\xi = 90^\circ$
Dir. [dB]	26.5	28.5
X-Pol [dB]	-41.4	-19.1
SLL [dB]	-19.1	-14.6
e_a [%]	20.6	31.7

(b)		
0.017 mm	$\xi = 0^\circ$	$\xi = 90^\circ$
Dir. [dB]	25.5	27.3
X-Pol [dB]	-25.3	-15.1
SLL [dB]	-16.9	-12.5
e_a [%]	16.0	24.3

the process that perforates the upper plate. The PPW has 458 slot pairs, then the last pairs of the spiral have $W_s = 0.7$ mm. Note that, the length is kept constant throughout the spiral with $L_s = \lambda_g/2$.

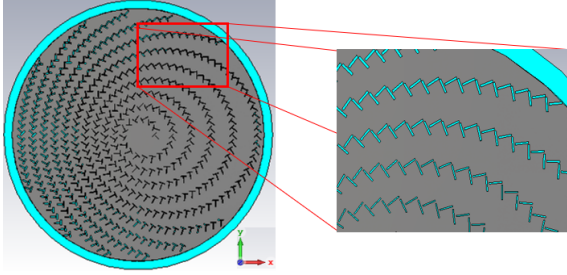


Fig. 15. Slot distribution for sub-spherical when slot width varies from [0.15,0.7] mm

The $S_{1,1}$ in both solutions have a return loss across the entire frequency band higher than 10 dB. From the CST results is not possible to evaluate correctly the best solution, hence we progress for an evaluation of the results with TA. The CST fields are extracted when plane z is 5 mm above the upper plate plane, and then applied on RLSA_TA script. Table V reveals the RLSA_Ta obtained for this test with the width varying.

From Table V, in both cases, either for $\xi = 0^\circ$ or $\xi = 90^\circ$, the aperture efficiency does not increase significantly, only around 3%. The X-pol increased slightly. In conclusion, varying the width of the pair of slots do not generate notably changes on the final results, but still presents better results, but not as expected.

Slot Length Variation

The increase of the slot length throughout the spiral is tested as proposed in several types of research, such as [9], [14], [19], keeping their width constant, $W_s = \lambda_g/20$. The logical reason is that the wave power decreases within the waveguide from the center to the edge of the PPW. The slot length should increase along the spiral to have a more even distribution over the aperture. As the previous subsection, when the length is

TABLE V
RLSA_TA RESULTS AT 30 GHZ FOR: W_s CONSTANT (A) W_s VARY (B)

(a)		
W_s constant	$\xi = 0^\circ$	$\xi = 90^\circ$
Dir. [dB]	25.5	27.3
X-Pol [dB]	-25.3	-15.1
SLL [dB]	-16.9	-12.5
e_a [%]	16.0	24.3

(b)		
W_s vary	$\xi = 0^\circ$	$\xi = 90^\circ$
Dir. [dB]	26.1	27.7
X-Pol [dB]	-29.1	-15.0
SLL [dB]	-18.4	-10.3
e_a [%]	18.2	26.6

varied, we must pay attention also to the critical zone. We want the slot length, L_s , to increase as much as possible, however, they must not overlap in the critical zone shown in Figure 16. Therefore, the maximum L_s of the furthest slot must be 3.60 mm. The first slot started with a L_s equal to 2.85 mm. After every 30 pairs of slots, the length increases by 50 μm , for the same reason as the slot width variation study. Also, for this study, both reflection coefficients are below -10 dB. RLSA_TA results should confirm which solution is more favorable. Table VI presents the maximum directivity, X-pol, SLL and the aperture efficiency when the $\xi = 0^\circ$ (a) and when $\xi = 90^\circ$ (b) for L_s constant and L_s vary.

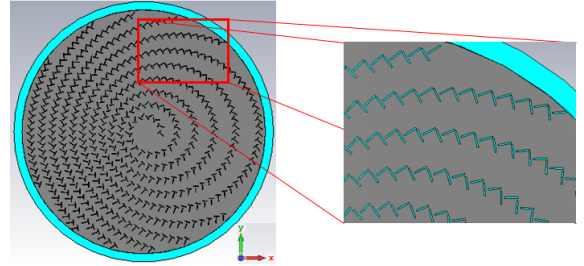


Fig. 16. Slot distribution for sub-spherical when slot varies from [2.85,3.60] mm

There is a clear improvement in increasing the length of slot pairs. Aperture efficiency and X-Pol increase. The SLL did not show much better results. Although the SLL has a slight increase, all other parameters have improved system performance. Scan loss is less than 3dB, SLL is also not a problem as it stays below -10dB, and efficiency increases, so the solution with varying slot length is more reliable. Also, comparing Table VI (b) with Table V (b), there is clearly a difference in term of aperture efficiency and X-Pol. A solution varying both width and length would be a complex challenge, because to increase them as possible, we need to make sure that the slots on the critical zone do not overlap.

IV. RLSA FINAL SETUP

For the final model, and according to the study throughout this work, we consider as a final design, a RLSA with a

TABLE VI
RLSA_TA RESULTS AT 30 GHZ FOR: L_s CONSTANT (A) L_s VARY (B)

(a)		
L_s constant	$\xi = 0^\circ$	$\xi = 90^\circ$
Dir. [dB]	25.5	27.3
X-Pol [dB]	-25.3	-15.1
SLL [dB]	-16.9	-12.5
e_a [%]	16.0	24.3

(b)		
L_s vary	$\xi = 0^\circ$	$\xi = 90^\circ$
Dir. [dB]	27.4	29.2
X-Pol [dB]	-32.0	-19.5
SLL [dB]	-15.8	-14.0
e_a [%]	24.8	37.2

matching spiral and an absorber rim surrounding the PPW and the matching spiral. For the aperture distribution, we choose the solution where the length of the slots increase throughout the spiral, and slot width is kept constant. The total number of pairs of unit radiators on the top plate is 458. Fig. 17 shows the reflection coefficient of the final design of CP-RLSA.

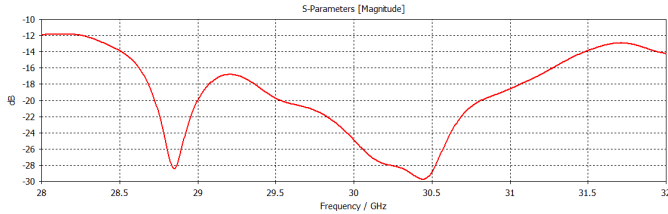


Fig. 17. $S_{1,1}$ for the final RLSA designed

The best results occur in [28.4; 30.1] GHz, which is a wide band for this type of antennas. The best results are chosen considering certain parameters. Every frequency that a result has a directivity equal to or less than 1 dB in relation to the maximum directivity is considered a good result. Also, X-Pol and SLL are less than -15 dB and -10 dB, respectively. Finally, if the scan loss is less than 3dB, it is a good result. The best performing frequency was 28.8 GHz. Table VII presents the RLSA_TA results for 28.8 GHz, while Fig. 18 illustrates de 3D radiation pattern directivity for 28.8 GHZ, when $\xi = 0^\circ$ (a) and $\xi = 90^\circ$ (b).

TABLE VII
RLSA_TA RESULTS FOR RLSA-DESIGN AT 28.8 GHZ

28.8 GHZ	$\xi = 0^\circ$	$\xi = 90^\circ$
Dir. [dB]	27.3	29.8
X-Pol [dB]	-28.3	-26.1
SLL [dB]	-13.3	-19.6
e_a [%]	26.2	46.5

V. CONCLUSIONS AND FUTURE WORK

This work is divided in two parts, where the first is mainly focused on a full-wave analysis of the antennas through CST

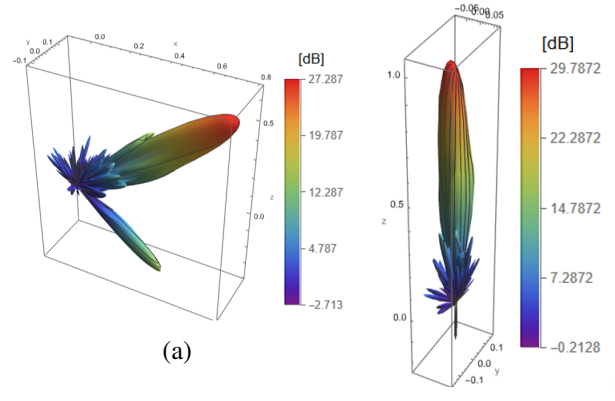


Fig. 18. RLSA_TA Farfield Directivity Radiation Pattern at 28.8 GHz for sub-spherical wave when $\xi = 0^\circ$ (a) and $\xi = 90^\circ$ (b)

and the second the Risley Prism concept is tested with the CP-RLSA and TA, that is placed above the antenna. Two antennas are designed to produce a collimated wave have a better frequency band of [28.5 GHz, 29.9] GHz. When the beam is boresight it has a peak directivity of 26.6 dBi at 29.5 GHz, while for a tilted beam the peak directivity of 26.4 dBi occurred at 29 GHz. Both presented a good return loss and SLL lower than -10 dB. The last antenna design emits a sub-spherical wave with a phase-shifting. Since it does not emit a collimated beam, a better study is made in the second part. The second part focuses on the phase distribution of the waves. Through the program RLSA_TA, the Risley prism is verified on the three designs, when an RLSA is used below a TA. However, for the last design, TA has a different phase distribution, correcting the phase of the sub-spherical wave, and performing a collimated beam from the antenna RLSA+TA. Once the new implementation is performing correctly, several types of structures and slots arrangement were studied with the lens, to obtain better results. For structures, we studied the use of a matching spiral in the bottom antenna plate, the utilization of an absorber around the edge of the RLSA to contain the reflections, and lastly a solution assembly the previous two solutions, with the absorber also surrounding the matching spiral. Regarding slot arrangement, it was studied a higher space between slot pairs, and an increment in their dimensions, either width or length, according to their radial distance. According to the results, as a final set up we have an RLSA antenna with an absorber and a matching spiral. The best slot arrangement was for an increment in the length of the slots along the spiral. The best results occurred for a frequency band of [28.8 GHz, 30.1] GHz, where all the frequencies n it had SLL < -10 dB, a X-pol < -15dB and scna loss lower than 3 dB.The antenna had a directivity peak of 29.8 dBi at 28.8 GHz for $\theta = 0^\circ$ in the elevation plane.

Some elements of the prototype designed in this work need an optimization and a depth studied. Starting with a better study about the dimensions of the matching spiral in the bottom plate of the antenna and the absorber that surrounds it. Also, the starting point of the matching spiral must be verified to get an even better antenna performance.

Lastly, the slot length interval increasing throughout the spiral, must have a depth study. The major problem remains in the aperture efficiency. One solution is a computational full-wave analysis based on MoM [7], [20]. Two other recent innovations presented regarding structure rather than slot optimization are very promising. The first proposal is to do an aggressive biased truncation of the slots distribution [21]. The remaining solution proposes to replace the dielectric material with a regular bed of metallic nails that acts as a slow-wave structure [22].

VI. ACKNOWLEDGEMENTS

This work was supported in part by FCT and under FEDER—PT2020 partnership agreement Project "ADAM3D" PTDC/EEI-TEL/30323/2017 - LISBOA-01-0145-FEDER-030323, and and Grant UID/EEA/50008/2020"

REFERENCES

- [1] F. Goebels and K. Kelly, "Arbitrarily polarized planar antennas," pp. 119–127, Mar. 2005, doi:10.1109/irecon.1959.1150781.
- [2] M. Ando, K. Sakurai, and N. Goto, "A Radial Line Slot Antenna for 12 GHz Band Satellite TV Reception," *IEEE Trans. Antennas Propag.*, vol. 34, no. 10, pp. 1269–1272, 1986, doi:10.1109/TAP.1986.1143744.
- [3] M. Ando, T. Numata, J. I. Takada, and N. Goto, "A Linearly Polarized Radial Line Slot Antenna," *IEEE Trans. Antennas Propag.*, vol. 36, no. 12, pp. 1675–1680, 1988, doi:10.1109/8.14389.
- [4] M. Ando, M. Takahashi, J. M. Natori, Takada, and N. Goto, "Single-layered radial line slot antenna for DBS reception," *Conference Proceedings - European Microwave Conference*, vol. 2, no. 20, pp. 1541–1546, 1990, doi:10.1109/euma.1990.336287.
- [5] M. Takahashi, M. Yoshiie, and M. Abe, "Basic design of beam tilting radial line slot antennas," *IEEE Trans. Antennas Propag. Soc. AP-S Int. Symp.*, vol. 2, pp. 1384–1387, 1995, doi:10.1109/aps.1995.530833.
- [6] M. V. Isasa, M. S. Castañer, and M. S. Pérez, "Design of circular polarized radial line slot antennas," *Int. J. Wirel. Opt. Commun.*, vol. 01, no. 02, pp. 179–189, 2003, doi:10.1142/s0219799503000161.
- [7] M. Albani, A. Mazzinghi, and A. Freni, "Automatic design of cp-rlsa antennas," *IEEE Trans. Antennas Propag.*, vol. 60, no. 12, pp. 5538–5547, 2012, doi:10.1109/TAP.2012.2214014.
- [8] M. N. Y. Koli, M. U. Afzal, K. Esselle, and M. Z. Islam, "Comparison between fully and partially filled dielectric materials on the waveguide of circularly polarised radial line slot array antennas," *2020 International Workshop on Antenna Technology (iWAT)*, pp. 1–3, 2020, doi:10.1109/iWAT48004.2020.1570609850.
- [9] M. N. Y. Koli, M. U. Afzal, K. Esselle, and R. M. Hashmi, "An all-metal high-gain radial-line slot-array antenna for low-cost satellite communication systems," in *IEEE Access*, vol. 8, pp. 139 422–139 432, 2020, doi:10.1109/ACCESS.2020.3012787.
- [10] M. J. Lopez-Morales, F. R. Varela, D. V. Vazquez, and M. S. Castaner, "Efficient design of radial line slot antennas using currents synthesis and optimization," *IEEE Antennas Wirel. Propag. Lett.*, vol. 19, no. 3, pp. 487–491, 2020, doi:10.1109/LAWP.2020.2966124.
- [11] M. U. Afzal and K. P. Esselle, "Application of near-field phase transformation to steer the beam of high-gain antennas in two dimensions," *2017 IEEE International Symposium on Antennas and Propagation USNC/URSI National Radio Science Meeting*, pp. 1947–1948, 2017, doi:10.1109/APUSNCURSINRSM.2017.8073016.
- [12] M. U. Afzal, K. P. Esselle, and M. N. Y. Koli, "A beam-steering solution with highly transmitting hybrid metasurfaces and circularly polarized high-gain radial-line slot array antennas," in *IEEE Transactions on Antennas and Propagation*, vol. 70, no. 1, pp. 365–377, Jan. 2022, doi:10.1109/TAP.2021.3111522.
- [13] Z. Zhang, Y. C. Zhong, H. Luyen, J. H. Booske, and N. Behdad, "A low-profile, risley-prism-based, beam-steerable antenna employing a single flat prism," in *IEEE Transactions on Antennas and Propagation*, Mar. 2022, doi:10.1109/TAP.2022.3161562.
- [14] M. U. Afzal, N. Y. Koli, and K. P. Esselle, "Low-cost radial line slot array antenna for millimeter-wave backhaul links," *2021 15th European Conference on Antennas and Propagation (EuCAP)*, pp. 1–4, 2021, doi:10.23919/EuCAP51087.2021.9411009.
- [15] C. A. Balanis, *Antenna Theory - Analysis and Design*, 4th ed. John Wiley Sons, 2016.
- [16] F. Faria, "User terminal planar antennas for wireless broadband access at ka satellite band," [Master's thesis, University of Lisbon], (2021), <https://fenix.tecnico.ulisboa.pt/cursos/meec/dissertacao/1128253548922054>.
- [17] N. Gagnon and A. Petrosa, "Using rotatable planar phase shifting surfaces to steer a high-gain beam," *IEEE Trans. Antennas Propag.*, vol. 61, no. 6, pp. 3086–3092, Jun. 2013, doi:10.1109/TAP.2013.2253298.
- [18] M. N. Y. Koli, M. U. Afzal, K. Esselle, and M. Z. Islam, "A high gain radial line slot array antenna for satellite reception," *2018 Australian Microwave Symposium (AMS)*, pp. 65–66, 2018, doi:10.1109/AUSMS.2018.8346984.
- [19] M. N. Y. Koli, M. U. Afzal, K. Esselle, L. Matekovits, and M. Z. Islam, "Investigating small aperture radial line slot array antennas for medium gain communication links," *2019 International Conference on Electromagnetics in Advanced Applications (ICEAA)*, pp. 0613–0616, 2019, doi:10.1109/ICEAA.2019.8879073.
- [20] J. I. Herranz-Herruzo, A. Valero-Nogueira, and M. Ferrando-Bataller, "Optimization technique for linearly polarized radial-line slot-array antennas using the multiple sweep method of moments," *IEEE Trans. Antennas Propag.*, vol. 52, no. 4, pp. 1015–1023, Apr. 2004, doi:10.1109/TAP.2004.825182.
- [21] M. N. Y. Koli, M. U. Afzal, and K. P. Esselle, "Increasing the gain of beam-tilted circularly polarized radial-line slot array antennas," in *IEEE Transactions on Antennas and Propagation*, 2022, doi:10.1109/TAP.2022.3140490.
- [22] J. I. Herranz-Herruzo, A. Valero-Nogueira, M. Ferrando-Rocher, and B. Bernardo-Clemente, "High-efficiency ka-band circularly polarized radial-line slot array antenna on a bed of nails," *IEEE Transactions on Antennas and Propagation*, vol. 70, no. 5, pp. 3343–3353, May. 2022, doi:10.1109/TAP.2021.3137376.